Journal of Colloid and Interface Science 487 (2017) 401–409

Contents lists available at ScienceDirect

Journal of Colloid and Interface Science

journal homepage: www.elsevier.com/locate/jcis

Effect of fluorine additive on $CeO_2(ZrO_2)/TiO_2$ for selective catalytic reduction of NO by NH_3

Qijie Jin [1], Yuesong Shen [1,*], Shemin Zhu [*]

College of Materials Science and Engineering, Nanjing Tech University, Nanjing 210009, China
Jiangsu Collaborative Innovation Center for Advanced Inorganic Function Composites, Nanjing Tech University, Nanjing 210009, China
Jiangsu National Synergetic Innovation Center for Advanced Materials, Nanjing Tech University, Nanjing 210009, China

GRAPHICAL ABSTRACT

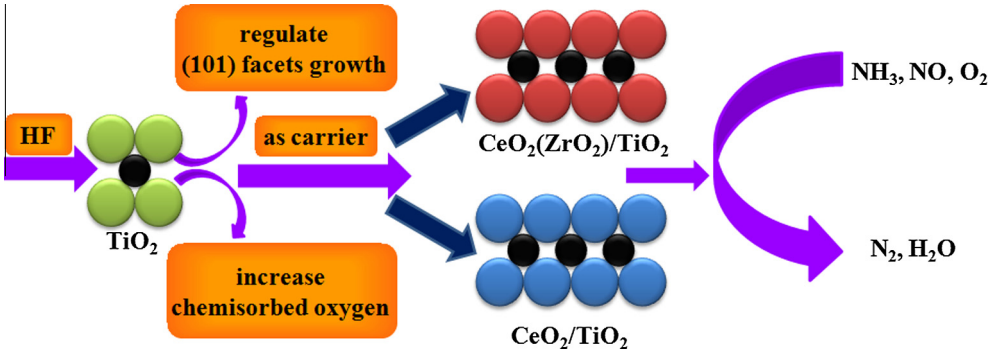

ARTICLE INFO

Article history:
Received 27 July 2016
Revised 19 October 2016
Accepted 20 October 2016
Available online 24 October 2016

Keywords:
$CeO_2(ZrO_2)/TiO_2$
Fluorine additive
Catalytic performance
Nitrogen oxide
Selective catalytic reduction

ABSTRACT

A series of $CeO_2(ZrO_2)/TiO_2$ catalysts with fluorine additive were prepared by impregnation method and tested for selective catalytic reduction (SCR) of NO by NH_3. These samples were characterized by XRD, N_2-BET, Raman spectra, SEM, TEM, NH_3-TPD, H_2-TPR and XPS, respectively. Results showed that the optimal catalyst with the appropriate HF exhibited excellent performance for NH_3-SCR and more than 96% NO conversion at 360 °C under GHSV of 71,400 h^{-1}. It was found that the grain size of TiO_2 increased and the specific surface area reduced with the modulation of HF, which was not good for the adsorption of gas molecule. However, the modulation of HF exposed the high energy (0 0 1) facets of TiO_2 and increased the surface chemisorbed oxygen concentration, oxygen storage capacity and Ce^{3+} concentration of catalyst. In addition, the synergy of (1 0 1) and (0 0 1) facets was beneficial to the improvement of catalytic activity.

1. Introduction

Nitrogen oxides (NO_x) are one of the major factors responsible for the worsening environment problems such as acid rain, photochemical smog and the greenhouse effect [1,2]. Denitrification has become an active demand to protect the ecological environment. Selective catalytic reduction of NO with NH_3 (NH_3-SCR) is the most widely employed technology for the abatement of the emission of

* Corresponding authors at: Jiangsu Collaborative Innovation Center for Advanced Inorganic Function Composites, State Key Laboratory of Materials-Oriented Chemical Engineering, College of Materials Science and Engineering, Nanjing Tech University, No. 5 Xinmofan Road, Nanjing 210009, China.
E-mail addresses: sys-njut@163.com (Y. Shen), szsm313@163.com (S. Zhu).
[1] These authors contributed equally to this work.

http://dx.doi.org/10.1016/j.jcis.2016.10.056
0021-9797/

NO. Currently, the most commercially used catalysts are $V_2O_5(WO_3, MoO_3)/TiO_2$ catalysts [3]. However, the operation temperature window of V_2O_5/TiO_2 catalysts is relatively narrow. Moreover, the V_2O_5-based catalyst still suffers from a low N_2 selectivity and sublimation of V_2O_5 at high temperatures even after modification with molybdenum and tungsten species [4,5]. Consequently, more and more attention has been given to develop environment-friendly NH_3-SCR catalysts with highly NO conversion and broad active temperature window.

Owing to its chemical inertness, long-term stability and environmental friendliness, TiO_2 has been applied in many fields, such as gas sensor application [6], coating [7] and photocatalysis [8]. For the NH_3-SCR, TiO_2 is often used as a catalyst carrier. In addition, CeO_2 is a widely used catalytic material because of its unique redox properties and high oxygen storage capacities, such as photocatalysis [9], fuel cell [10] and oxygen permeation membrane [11]. Based on the above reasons, many ceria-based catalysts have been developed, such as CeO_2/TiO_2 [12,13], Ce-W-O_x/TiO_2 [14–16], CeO_2/TiO_2-SiO_2 [17,18], Ce-Zr-O_x/TiO_2 [19,20], Mn-Ce-O_x/TiO_2 [21–24] and so on. These catalysts could show effective denitration activity in a wide active temperature window.

Many previous researches have been proved that the fluorine additive can enhance the catalytic activity for NH_3-SCR [25–27]. In addition, Many theoretical and experimental studies have been developed to control the growth of different TiO_2 crystal faces, and the modulation of HF can expose the (0 0 1) facets. For anatase TiO_2, it has been found that the order of the average surface energies is $\gamma(1\,1\,0) > \gamma(0\,0\,1) > \gamma(1\,0\,0) > \gamma(1\,0\,1)$ [28]. In other words, the anatase TiO_2 with (0 0 1) facets are more reactive than the (1 0 1) facets, which is favorable to the increase of catalytic performance in many fields. Therefore, the exposure of TiO_2 crystal faces can be regulated with the modulation of HF, and the HF modified TiO_2 will be used as a catalyst carrier, which might enhance the catalytic activity of $CeO_2(ZrO_2)/TiO_2$ (CZT for short) catalysts theoretically. Based on the previous researches of our team, the aim of this work is to explore the rule for effect of fluorine additive on catalytic activity in the CZT catalysts.

2. Experiment

2.1. Catalyst preparation

TiO_2 with the modulation of HF was prepared by a hydrothermal method. In a typical preparation, the appropriate HF solution (concentration: 40 wt.%), 10 mL distilled water and 50 mL Ti $(OC_4H_9)_4$ were mixed together in a 100 mL Teflon-lined autoclave, and then kept at 180 °C for 24 h. The resulting white precipitate was washed three times with ethanol and distilled water. The residual solid was dried at 80 °C for 6 h and then calcined at 500 °C for 2 h. The added contents of HF were 0 mL, 5 mL, 10 mL and 15 mL, respectively.

The molar ratio of Ti:Ce:Zr (when used) in the catalyst was designed as 4:1:1. The TiO_2 supports were dipped in the mixed aqueous solution of $ZrOCl_2{\cdot}8H_2O$ and $Ce(NO_3)_3{\cdot}6H_2O$, and the mixed solution was stirred for 2 h at room temperature. Then the product was followed by drying in air at 80 °C for 24 h and the solid was calcined at 500 °C for 2 h. The catalysts were designated as CT-XF and CZT-XF (X = 0, 5, 10 and 15), respectively.

2.2. Catalytic activity and selectivity measurement

The catalytic activity measurements of the prepared catalysts for NH_3-SCR of NO were carried out in a fixed-bed quartz reactor (6 mm inner diameter), with 0.7 mL catalysts (particle sizes of 0.3–0.45 mm) and 833 mL min^{-1} gas flow rate corresponding to a GHSV of 71,400 h^{-1}. The reactant gas typically consisted of 600 ppm NO, 600 ppm NH_3, 6% O_2 and balance N_2. The NO concentrations at the inlet and outlet of the reactor were monitored online by a flue gas analyzer (MRU VarioPlus, Germany). The catalytic activity (X_{NO}) for NH_3-SCR of NO was expressed by Eq. (1). The analysis at each selected temperature was performed after 30 min since the reactor temperature was stabilized.

$$X_{NO} = ([NO]_{inlet} - [NO]_{outlet})/[NO]_{inlet} \times 100\% \quad (1)$$

The temperature range in which the catalytic activities were equal to or more than 90% of the maximum catalytic activity was defined as the catalytically active temperature window, expressed as T_r. The lowest temperature of T_r was named T_r-L, and the highest is named T_r-H.

The N_2 concentration at the outlet of the reactor was monitored on-line by a gas chromatography (GC2014, Japan), using a 5 Å molecular sieve column (2 m in length, sorbent particle sizes disperse from 60 mesh to 80 mesh), and a single-point corrected external standard method was adopted. The concrete GC detecting conditions were described as follows: injection volume was 1 mL, injector temperature was 90 °C, chromatographic column temperature was 80 °C, TCD detector was used at 120 °C, carrier gas was argon, hydrogen was 30 mL min^{-1}. Firstly we obtained the peak area of the known standard N_2/Ar (600 ppm, and balance Ar) and defined the area as S_0, and then we obtained the peak area of the detected N_2 at the outlet and defined the area as S. According to the following reaction:

$$4NH_3 + 4NO + O_2 \rightarrow 4N_2 + 6H_2O \quad (2)$$

Thus, the NO_x concentration merely consumed by N_2: $[NO_x]_{N2consu} = [N_2] = 600\,S/S_0$ ppmv, while the total concentration of NO_x conversion: $[NO_x]_{conv}=[NO_x]_{inlet}-[NO_x]_{outlet}$. In order to facilitate the quantitative analysis and discussed the N_2 selectivity of the catalysts for NH_3-SCR of NO_x, the N_2 selectivity for NH_3-SCR of NO_x was expressed by Eq. (3):

$$\eta = [NO]_{N2consu}/[NO]_{conv} \times 100\% = 600S/(S_0[NO]_{inlet} - S_0[NO]_{outlet}) \times 100\% \quad (3)$$

2.3. Characterization

Powder X-ray diffraction (XRD) patterns were obtained on the X-ray diffractometer (Smartlab TM 9Kw, Rigaku, Japan) using Cu Kα radiation. The 2θ scans covered the range 10–80°, and the accelerating voltage and applying current were 45 kV and 200 mA, respectively. The microstructural natures of the catalysts have been investigated using a scanning electron microscope (JEOL, JSM-5900) and transmission electron microscopy (JEOL, JEM-2010UHR). The AXIS ULTRA DLD instrument was used for X-ray photoelectron spectroscopy (XPS) analysis, and monochromatic Al-Kα radiation was used as the excitation source. After complete removal of moisture from the catalysts by drying at 100 °C for 24 h, the catalysts were analyzed without surface sputtering or etching so that the degree of vacuum in the XPS equipment was maintained at 10^{-7} Pa. Visible Raman spectra of the catalysts were collected at room temperature on the LabRAMHR800 (Horiba Jobin Yvon). A 514 nm diode-pumped solid-state semiconductor laser was used as the excitation source with a power output of 30 mW.

The number of acidic sites and acid strength of the catalysts were evaluated by a temperature programmed desorption (TPD) of ammonia using CHEMBET-3000 (Quantachrome). The samples were preheated to 450 °C under a helium stream for 1 h, and then cooled to 100 °C for ammonia adsorption. Then ammonia was desorbed using helium at a flow rate of 30 mL min^{-1} from 100 °C to 800 °C at a heating rate of 10 °C min^{-1}. The ammonia desorption

was monitored online by a Thermo ONIX ProLab mass spectrometer. The H_2-TPR was performed on a Semiautomatic Micromeritics TPD/TPR 2900 apparatus. The samples were pre-treated, before the reduction measurement, at 400 °C for 1 h in an argon flow, and then cooled to 50 °C. Reduction profiles were obtained by passing a 5% H_2/Ar flow at the flow rate of 20 mL min^{-1}. The temperature was increased from 50 °C to 900 °C at the rate of 10 °C min^{-1}. The specific surface area and average pore diameter (BET method) of the samples were measured by N_2 adsorption/desorption isotherms at 77 K using a surface area analyzer (Micromeritics, 2020 M V3.00H). All the samples were degassed at 350 °C under vacuum for 3 h prior to the adsorption experiments.

3. Results and discussion

3.1. Catalytic performance

Fig. 1 displayed the temperature dependence of NO conversion obtained with the different catalysts. As shown in Fig. 1(a), the TiO_2-0F showed the maximum catalytic activity (22.0%) at 400 °C and the addition of HF led to an obvious enhancement of the activity. The maximum catalytic activity decreased in the following order TiO_2-10F > TiO_2-5F > TiO_2-15F > TiO_2-0F. The catalytic activity decreased with excess HF, which may due to too much amount of (0 0 1) facets. Fig. 1(b) showed the catalytic activity of CT catalysts. The maximum catalytic activity of CT-0F was 90.1% and the catalytically active temperature window was 330–430 °C. As shown in Fig. 1(b), the catalytic activity increased slightly with the small additions of HF and the CT-10F showed the highest activity (95.6%) and the widest catalytically active temperature window (315–445 °C). In addition, the catalytic activity of CT-15F was lower than that of CT-0F, indicating that the excess HF was not beneficial for the catalytic activity. Fig. 1(c) showed comparison of catalytic activity of CZT catalysts. The modulation of HF corresponded to similar law, but different slightly. The maximum catalytic activity of CZT-10F was 96.5% at 360 °C, while that of CZT-0F was 93.4% at 400 °C. In addition, the catalytic activity decreased slightly with the modulation of HF when reaction temperature was higher than 420 °C. The maximum catalytic activity decreased in the following order CZT-10F > CZT-5F > CZT-0F > CZT-15F, indicating that the suitable addition of HF could increase the catalytic activity significantly.

As shown in Fig. 1, all of the catalytic activity curves showed a parabolic trend as the reaction temperature increased: the catalytic activity increased at temperatures lower than the T_r-L, which may result from that the quantity of activated molecules and the effective collision frequency on the surface of the catalysts increased with the increase of temperature [29]. In addition, ammonia oxidation occurred at temperatures higher than the T_r-H, which directly reduced the content of reducing agent, so that the catalytic activity decreased gradually. At the last, Fig. 2 presented the N_2 selectivity of CT and CZT catalysts for NH_3-SCR of NO at different temperatures. There was no great difference of N_2 selectivity when HF was used for the modulation of crystal growth in different directions. In addition, the N_2 selectivity of CT increased slightly with the addition of Zr element, which was similar with the result of our previous work [30].

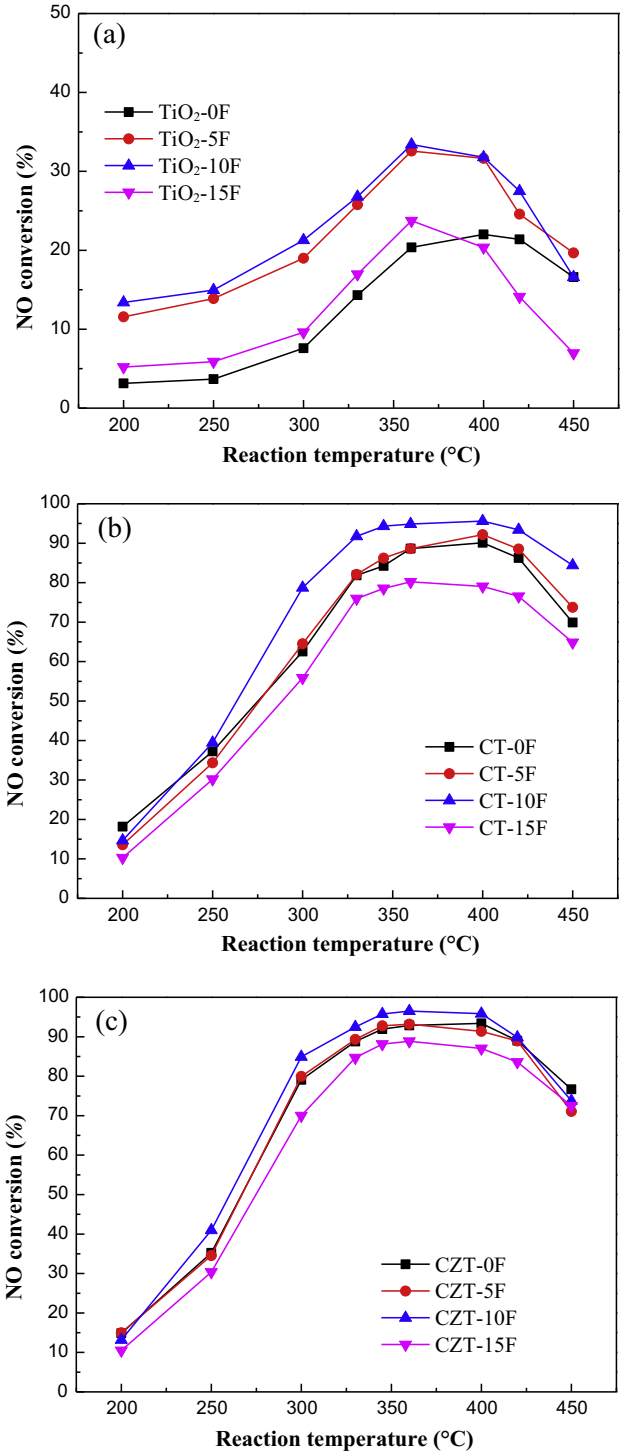

Fig. 1. NO conversion in the NH_3-SCR reaction over (a) TiO_2; (b) CT and (c) CZT catalysts. Reaction conditions: 600 ppm NO, 600 ppm NH_3, 6% O_2 in N_2, at a GSHV of 71,400 h^{-1}.

3.2. XRD and BET analysis

The XRD results of different catalysts were showed in Fig. 3. All the reflections of the CZT catalysts provided typical diffraction patterns for the anatase TiO_2 (2θ = 25.2°, 37.5°, 47.8°, 53.5°) (PDF-ICDD 71-1168), CeO_2 (2θ = 28.6°, 33.1°, 47.5°, 56.4°) (PDF-ICDD 65-5923) and $Ce_{0.75}Zr_{0.25}O_2$ (2θ = 28.8°, 33.5°, 48.1°) (PDF-ICDD 28-271). As shown in Fig. 3, the three strong peaks of TiO_2 at 2θ = 25.2°, 37.5°, 47.8° were attributed to anatase (1 0 1), (004) and (2 0 0) diffractions, respectively. The intensity of the diffraction peaks, especially the (1 0 1) and (2 0 0), increased obviously with the modulation of HF. As well known, the number of TiO_2 crystal nucleus reduced seriously when $Ti(OH)_4$ reacted with HF and HF could control the grain growth of TiO_2 [28]. Therefore, the grain size of TiO_2 would increase with the modulation of HF, which resulted in the increase of diffraction peak intensity.

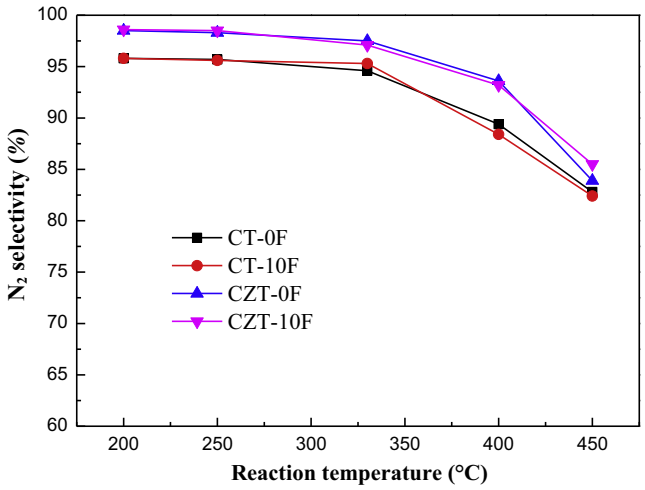

Fig. 2. N_2 selectivity in the NH_3-SCR reaction over different catalysts.

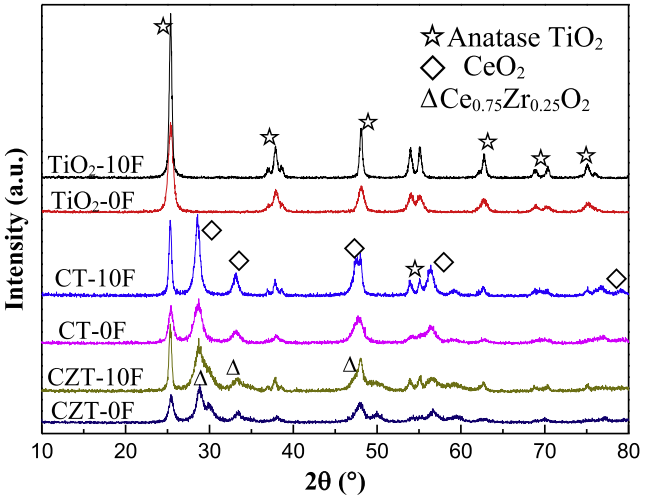

Fig. 3. X-ray diffraction patterns of (a) TiO_2; (b) CT and CZT catalysts.

After the doping of ceria and zirconia, the peaks of ceria and ceria-zirconia solid solution were observed obviously in the spectra of the catalysts. In addition, the diffraction peaks of CT-0F and CZT-0F samples were broader than those for the CT-10F and CZT-10F, indicating that CT-0F and CZT-0F have smaller crystallite sizes. That was because HF, as a facet-controlling agent, would lead to the growth of particles to larger plates [31,32]. The change of crystallite sizes may affect the catalytic performance of CZT catalyst.

The specific surface areas of the samples were summarized in Table 1. The surface areas of TiO_2-0F and TiO_2-10F were 103.98 $m^2\,g^{-1}$ and 35.82 $m^2\,g^{-1}$, respectively. As well known, it was very easy to take the fusion of neighbor TiO_2 along the (0 0 1) direction so that the surface energy could minimize [33]. On the other hand, the increase of TiO_2 crystallite size would also reduce the specific surface area. Consequently, the specific surface area of TiO_2 decreased seriously with excess HF additive. In addition, both the addition of Ce also reduced the specific surface area of TiO_2, which could result from the plugging of TiO_2 porous channels. Furthermore, the specific surface area decreased as CZT-0F > CT-0F and CZT-10F > CT-10F, indicating that the structure was more loose with the addition of Zr addition.

Table 1
Physical properties of different catalysts sample.

Sample	TiO_2-0F	TiO_2-10F	CT-0F	CT-10F	CZT-0F	CZT-10F
S_{BET} ($m^2\,g^{-1}$)	103.98	35.82	59.22	32.51	59.31	44.05

3.3. SEM and TEM analysis

Fig. 4 showed SEM micrographs of TiO_2-0F, TiO_2-10F, CT-0F, CT-10F, CZT-0F and CZT-10F with magnification times of 10,000. The congeries of TiO_2-0F was composed of many small particles, which resulted in the loose structure and the increase of porous channels. On the other hand, the structure of TiO_2-10F was compact and the pore structure evolved into slit shape, which might resulted from the fusion of neighbor TiO_2 along the (0 0 1) direction. After the doping of ceria, the particles of CT catalysts grew completely and the addition of Zr addition led to the more loose structure. In addition, Figs. S1–S4 showed the elemental mapping characterization of different catalysts and explained the distribution of different elements. As shown in Figs. S1–S4, the Ti, Ce, Zr and O elements were well distributed on the catalysts surface.

Figs. 5 and 6 showed HR-TEM images of TiO_2-0F and TiO_2-10F. The average size of TiO_2-10F (15–20 nm) was much larger than that of TiO_2-0F (5–10 nm), which corresponded to the XRD result. In addition, the lattice fringes with an interplanar spacing of 0.35 nm and 0.235 nm were consistent with the d-spacing of (1 0 1) and (0 0 1) facets, respectively [34,35]. The main reason for the high exposed (0 0 1) facets was the addition of HF in the precursor solutions, where the adsorbed F anions increased the relative stabilities of (0 0 1) facets [36].

3.4. Raman spectra analysis

Visible Raman spectra were applied to characterize the catalysts, and the results were presented in Fig. 7. In the Raman spectra, the four peaks were assigned to the anatase crystalline phase, which could be observed at 146, 398, 518 and 640 cm^{-1}. The band located at 466 cm^{-1} was assigned to the symmetric vibration of CeO_2 [37]. As shown in Fig. 7, the Raman spectral intensity of 146 and 640 cm^{-1} band increased with the modulation of HF, which could be due to the stronger crystallinity of TiO_2-10F.

After the doping of ceria and zirconia, the Raman spectra demonstrated that CT and CZT catalysts showed a positive shift by about 1 or 2 cm^{-1} in comparison with TiO_2. In addition, the band of CeO_2 also shifted about 2 cm^{-1} compared with the standard value 464 cm^{-1}. The shift corresponded to an increase in the number of surface oxygen vacancies [38]. Moreover, the Raman spectral intensity of CeO_2 decreased significantly with the addition of Zr element, which could be due to the generation of $Ce_{0.75}Zr_{0.25}O_2$. This assumption could be proved in the XRD analysis. At the last, the Raman spectral intensity of anatase TiO_2 decreased as CT-10F > CT-0F and CZT-10F > CZT-0F, indicating that the crystallinity of catalyst would be stronger with the modulation of HF.

3.5 NH_3-TPD and H_2-TPR analysis

It was generally known that the acidity of catalyst could play an important role in the adsorption capacity of NH_3 for the sample [39]. Fig. 8 showed the NH_3-TPD profiles of different catalysts. All of the ammonia desorption of the catalysts displayed one broad desorption peak spanned at 100–500 °C represented the weak and medium acid sites [40]. The areas of NH_3-TPD profile decreased as CZT-10F≈CZT-0F > CT-10F ≈ CT-0F > TiO_2-10F ≈ TiO_2-0F, implying that the number of the acid sites decreased in the same order. That was to say, the high energy facets had no advantage for the adsorption of NH_3 [28]. In addition, the number

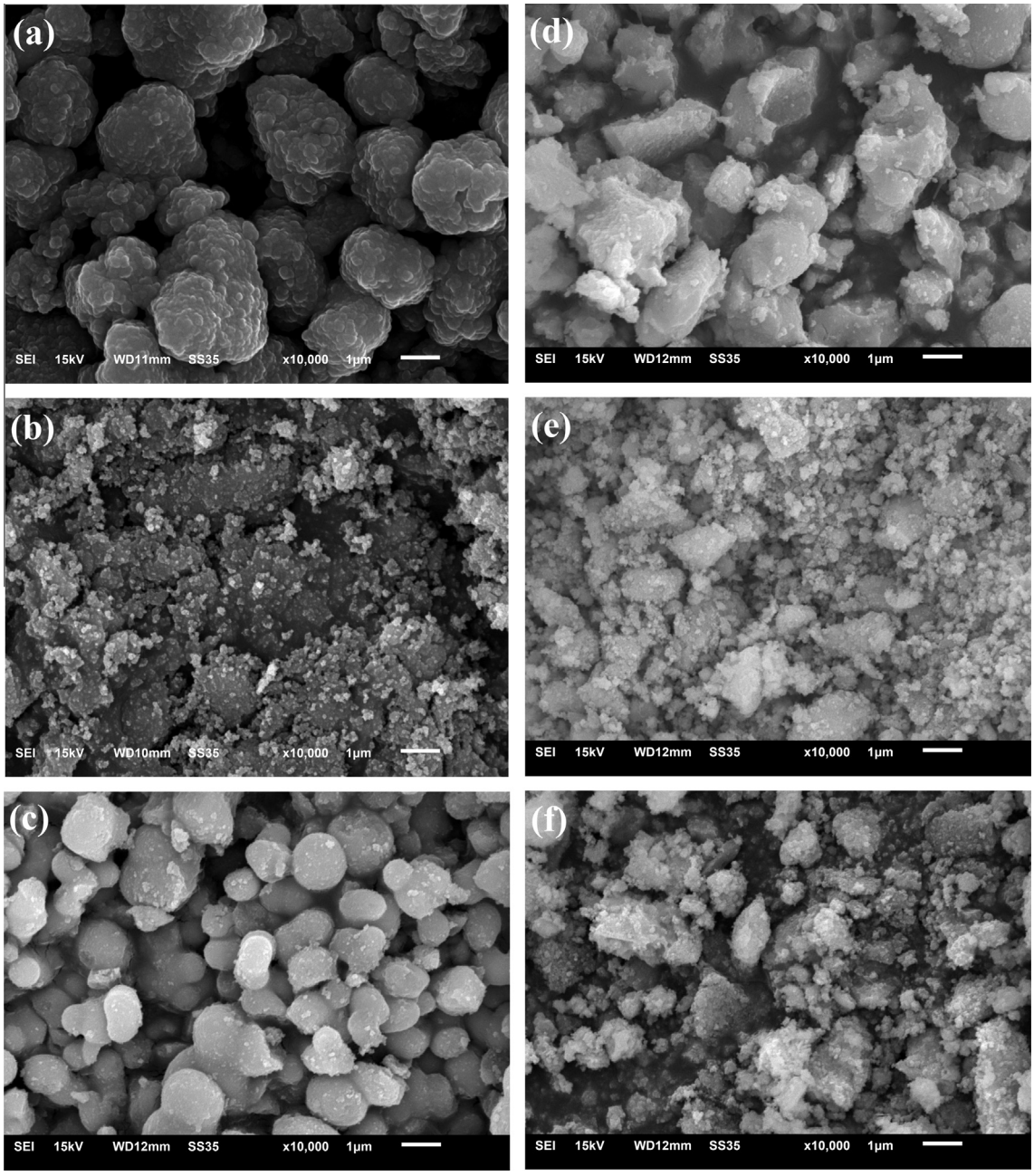

Fig. 4. SEM micrograph of (a) TiO_2-0F; (b) TiO_2-10F; (c) CT-0F; (d) CT-10F; (e) CZT-0F and (f) CZT-10F with magnification times of 10,000.

of the acid sites for TiO_2 catalyst increased obviously with the addition of Ce and Zr, which resulted in the increase of catalytic activity.

Fig. 9 showed the H_2-TPR results of different catalysts to evaluate the redox properties. For TiO_2-0F, two weak peaks centered at 540 °C and 591 °C were detected and only a broad peak located at 625 °C was observed obviously with the modulation of HF. In other words, the redox properties of TiO_2 decreased slightly with high energy facets. In addition, the reduction peaks shifted to the lower temperature after the doping of ceria. It revealed the improvement of redox properties with the addition of ceria. Furthermore, the CZT-0F catalyst presented three broad peaks. The broad peak centered at 444 °C was likely assigned to the reduction of surface oxygen of Ce^{4+}-O-Ce^{4+} [41,42]. The peak centered at 614 °C was attributed to the reduction of TiO_2 and surface oxygen of Ce^{3+}-O-Ce^{4+} [43,44]. The third peak centered at 753 °C corresponded to the reduction of bulk ceria because the reduction could only be taken place above 750 °C [45]. The reduction peaks of CZT-10F shifted to the lower temperature, which revealed the improvement of redox properties with the modulation of HF. Moreover, integral areas of the H_2-TPR profiles were usually calculated to compare the oxygen storage capacity of catalysts, which was a significant parameter to the SCR activity of ceria-based catalysts [46]. The total H_2 consumption decreased in the order CZT-10F > CZT-0F > TiO_2-10F > TiO_2-0F, suggesting that the oxygen storage capacity could be enhanced with the modulation of HF.

3.6. XPS analysis

Fig. 10 showed the O 1*s* XPS spectra of different catalysts. The O 1*s* peaks could be fitted into two peaks referred to the chemisorbed oxygen (hereafter denoted as O_α) and the lattice oxygen

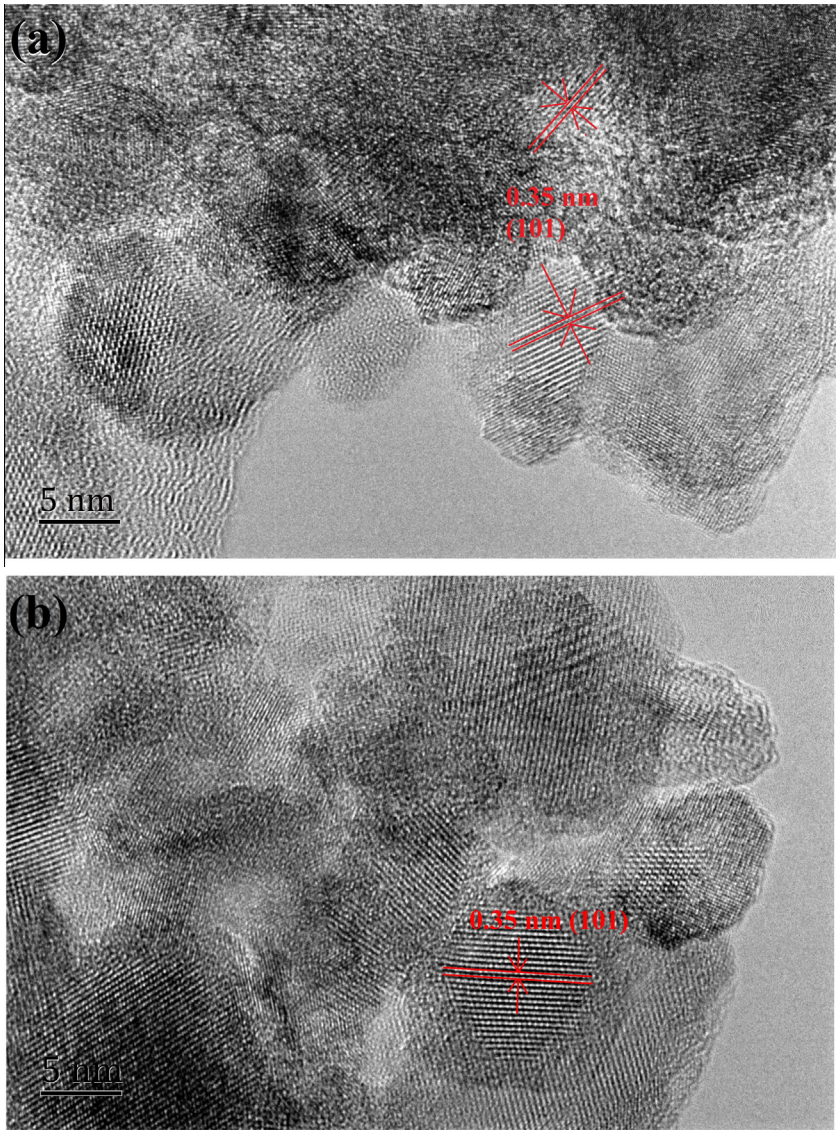

Fig. 5. HR-TEM images of TiO_2-0F.

(hereafter denoted as O_β) [45]. The O 1*s* core levels of TiO_2 shift to higher binding energy while that of CT and CZT catalysts shift to lower binding energy with the modulation of HF. The difference may result from the interaction of Ce and O atoms. In addition, there was the strong interaction of Ce, Zr and Ti atoms so that the O 1*s* peaks of TiO_2 showed a shift toward the lower binding energy with the addition of Ce and Zr. As shown in Fig. 11, the Ti 2*p* could be divided into two contributions of Ti^{3+} and Ti^{4+} [47]. The change of binding energy corresponded to similar law that the modulation of HF resulted in the positive shift and the negative shift resulted from the addition of Ce and Zr. By comparing with the intensity of Ti 2*p*, which of CT and CZT decreased obviously, indicating that the amount Ti of catalyst surface decreased with the addition of Ce and Zr. Fig. 12 showed the Ce 3*d* XPS spectra of CT-0F, CT-10F, CZT-0F and CZT-10F catalysts. All the spectral peaks could be observed at binding energies of 903 eV and 884 eV [48]. Therefore, the Ce 3*d* spectra could be ascribed to Ce^{4+} and Ce^{3+}. In addition, the intensity of Ce 3*d* peaks decreased as CT-10F > CZT-10F > CT-0F > CZT-0F. It was suggested that the amount Ce of catalyst surface decreased with the addition of Zr and the Ce was easier to expose on the catalyst surface with the modulation of HF. The Ti 2*p* core levels shifted to higher binding energy, indicating that the interactions among O and Ti increased slightly and the F has entered into TiO_2 lattice with the modulation of HF. In addition, the peaks of Ce and O showed a shift toward the lower binding energy with the modulation of HF, which indicated that the interaction decreased slightly.

Table 2 showed the atomic concentration of TiO_2, CT and CZT catalysts. The O_α atomic ratios of TiO_2-0F catalyst surface was 0.26 while that of the catalysts increased generally whether the addition of Ce, Zr or HF. On the contrary, the Ti^{3+} of atomic ratios decreased slightly in the mass when the HF, Ce or Zr was added into the catalyst. Surface chemisorbed oxygen has been reported to be the most active oxygen and played an important role in oxidation [49]. It meant that TiO_2-10F, CT-10F and CZT-10F might have better activity for the oxidation of NO, which was beneficial for the increase of catalytic activity. Furthermore, the atomic ratio of Ce^{3+} on the surface of CT-0F, CT-10F, CZT-0F and CZT-10F were 0.20, 0.21, 0.20 and 0.22 respectively. In other words, the addition of Zr was not beneficial while the modulation of HF was good for the increase of Ce^{3+}. The increase of Ce^{3+} on CT-10F and CZT-10F catalysts surface could be considered as one of the reasons for the increase of catalyst activity [16].

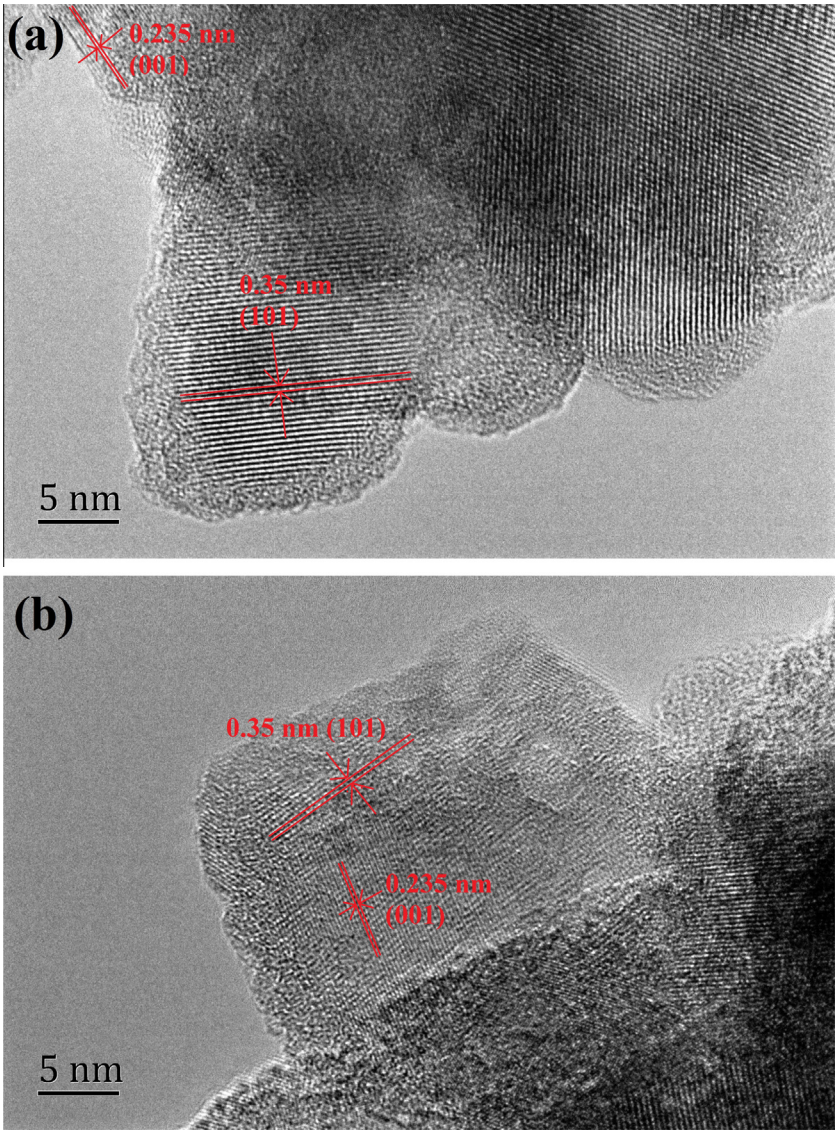

Fig. 6. HR-TEM images of TiO_2-10F.

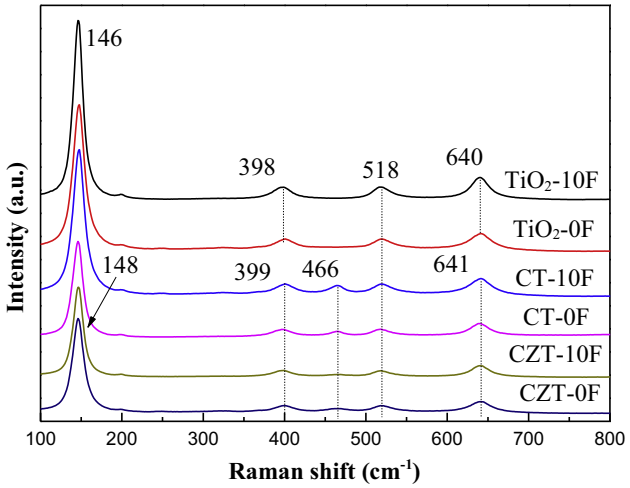

Fig. 7. Raman spectra of (a) TiO_2; (b) CT and CZT catalysts.

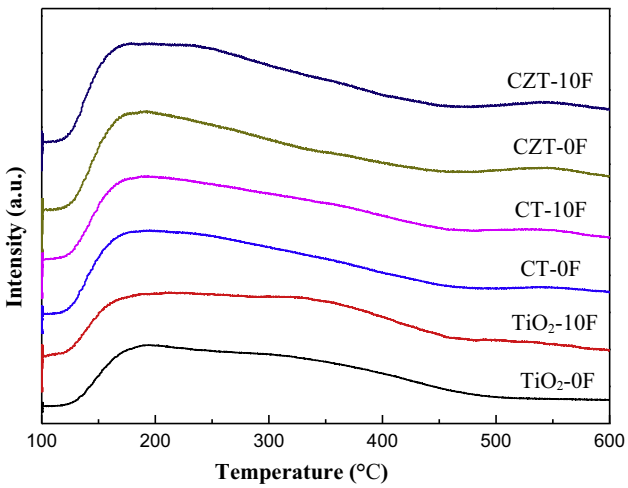

Fig. 8. NH_3-TPD profiles of different catalysts.

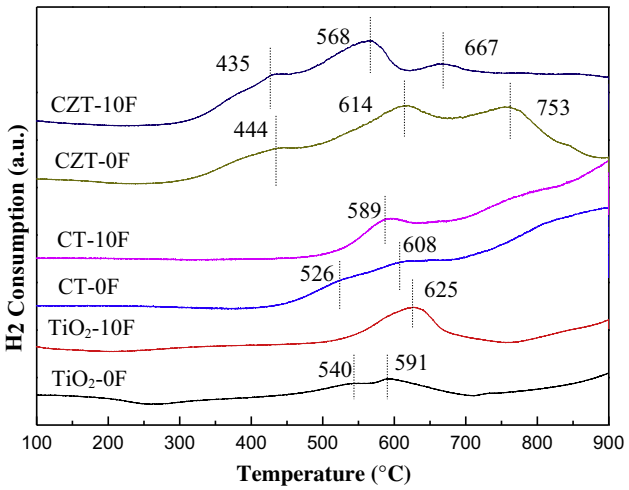

Fig. 9. H_2-TPR profiles of different catalysts.

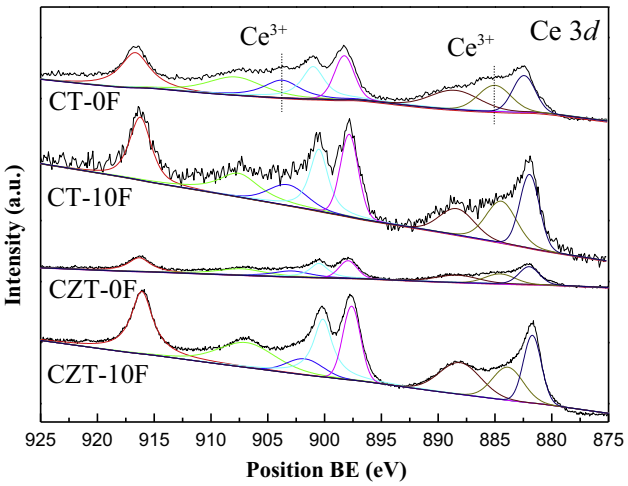

Fig. 12. Ce 3*d* XPS high-resolution scans spectra of different catalysts.

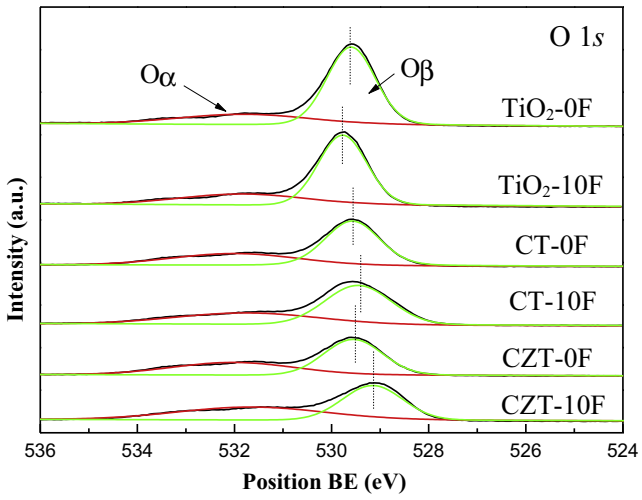

Fig. 10. O 1*s* XPS high-resolution scans spectra of different catalysts.

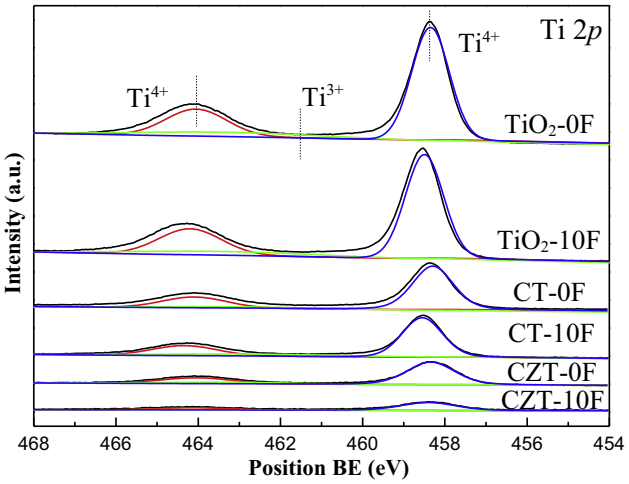

Fig. 11. Ti 2*p* XPS high-resolution scans spectra of different catalysts.

3.7. Discussion

Anyway, (0 0 1) and (1 0 1) facets have strong synergy and have been demonstrated as oxidative and reductive sites, respectively [50]. For the NH_3-SCR, the NO oxidation to form nitrate at the catalyst surface was a significant step so that the modulation of HF played an important role in the improvement of catalytic activity. In addition, the redox properties could be enhanced because of the synergy of low-energy (1 0 1) and high-energy (0 0 1) facets, which was also the reason why the catalytic activities of catalyst increased with the modulation of HF.

Although the specific surface area of catalyst decreased obviously when the HF was added to control the grain size of TiO_2, the suitable HF could also improve the catalytic activity of NH_3-SCR. That might because the adsorption of gas molecule was not the major factor for SCR. Moreover, the oxygen storage capacity of catalyst could also be enhanced with the modulation of HF, which was beneficial to improve catalytic activities. The concentrations of chemisorbed oxygen and Ce^{3+} on the catalyst surface increased with the modulation of HF. These reasons were conductive to obtain the excellent catalytic activity.

Table 2
Atomic ratios of different catalysts surface.

Samples	$O_\alpha/(O_\alpha + O_\beta)$	$Ti^{3+}/(Ti^{3+} + Ti^{4+})$	$Ce^{3+}/(Ce^{3+} + Ce^{4+})$
TiO_2-0F	0.26	0.17	–
TiO_2-10F	0.30	0.16	–
CT-0F	0.37	0.16	0.20
CT-10F	0.39	0.16	0.21
CZT-0F	0.43	0.13	0.20
CZT-10F	0.48	0.11	0.22

4. Conclusions

In this work, TiO_2 with the modulation of HF was synthesized by a hydrothermal method, and then used as catalyst carrier to study the effect of the HF additive on the $CeO_2(ZrO_2)/TiO_2$ for NH_3-SCR. It was found that (0 0 1) facets were exposed on the catalyst surface with the modulation of HF. With the appropriate HF, the grain size of TiO_2 increased and the specific surface area reduced. However, the oxygen storage capacity of catalyst could also be enhanced with the modulation of HF. In addition, the synergy of (1 0 1) and (0 0 1) facets and the increase of surface chemisorbed oxygen and Ce^{3+} concentrations were beneficial to the improvement of catalytic activity. With these superior capabilities, CZT-10F exhibited excellent catalytic performance for NH_3-SCR and more than 96% NO conversion at 360 °C under GHSV of 71,400 h^{-1}.

Acknowledgements

This work was supported by the National Natural Science Foundation of China (51272105), Jiangsu Provincial Science and Technology Supporting Program (BE2013718), National Key Research and Development Program of China (2016YFC0205500), Project Funded by the Priority Academic Program Development of Jiangsu Higher Education Institutions (PAPD).

Appendix A. Supplementary material

Supplementary data associated with this article can be found, in the online version, at http://dx.doi.org/10.1016/j.jcis.2016.10.056.

References

[1] L. Qu, C.T. Li, G.M. Zeng, M.Y. Zhang, M.F. Fu, J.F. Ma, F.M. Zhan, D.Q. Luo, Chem. Eng. J. 242 (2014) 76–85.
[2] J.H. Chen, F.F. Cao, R.Y. Qu, X. Gao, K.F. Cen, J. Colloid Interface Sci. 456 (2015) 66–75.
[3] X.L. Weng, X.X. Dai, Q.S. Zeng, Y. Liu, Z.B. Wu, J. Colloid Interface Sci. 461 (2016) 9–14.
[4] C.J. Tang, H.L. Zhang, L. Dong, Catal. Sci. Technol. 6 (2016) 1248–1264.
[5] X. Zhao, L. Huang, H.R. Li, H. Hu, J. Han, L.Y. Shi, D.S. Zhang, Chinese J. Catal. 36 (2015) 1886–1899.
[6] L.N. Appelhans, P.S. Finnegan, L.T. Massey, T.S. Luk, M.A. Rodriguez, M.T. Brumbach, B. McKenzie, J.M. Craven, Sensors Actuators, B: Chem. 228 (2016) 117–123.
[7] L.C. Córdoba, M.F. Montemor, T. Coradin, Corros. Sci. 104 (2016) 152–161.
[8] S.N. Xiao, W. Zhu, P.J. Liu, F.F. Liu, W.R. Dai, D.Q. Zhang, W. Chen, H.X. Li, Nanoscale 8 (2016) 2899–2907.
[9] M. Zeng, Y.Z. Li, M.Y. Mao, J.L. Bai, L. Ren, X.J. Zhao, ACS Catal. 5 (2015) 3278–3286.
[10] J. Kugai, E.B. Fox, C. Song, Appl. Catal. A: Gen. 456 (2013) 204–214.
[11] X. Yin, L. Hong, Z.L. Liu, J. Membr. Sci. 268 (2006) 2–12.
[12] J. Ding, Q. Zhong, S.L. Zhang, Ind. Eng. Chem. Res. 54 (2015) 2012–2022.
[13] Q. Li, H.C. Gu, P. Li, Y.H. Zhou, Chinese J. Catal. 35 (2014) 1289–1298.
[14] D.W. Kwon, K.B. Nam, S.C. Hong, Appl. Catal. A: Gen. 497 (2015) 160–166.
[15] W.P. Shan, F.D. Liu, H. He, X.Y. Shi, C.B. Zhang, Appl. Catal. B: Environ. 115–116 (2012) 100–106.
[16] L. Chen, J.H. Li, M.F. Ge, R.H. Zhu, Catal. Today 153 (2010) 77–83.
[17] C.X. Liu, L. Chen, J.H. Li, L. Ma, H. Arandiyan, Y. Du, J.Y. Xu, J.M. Hao, Environ. Sci. Technol. 46 (2012) 6182–6189.
[18] W.R. Zhao, Y. Tang, Y.P. Wan, L. Li, S. Yao, X.W. Li, J.L. Gu, Y.S. Li, J.L. Shi, J. Hazard. Mater. 278 (2014) 350–359.
[19] Y.S. Shen, S.M. Zhu, Catal. Sci. Technol. 2 (2012) 1806–1810.
[20] W.L. Fu, Y.S. Shen, S.M. Zhu, S.B. Shen, J. Inorg. Mater. 29 (2014) 1294–1300.
[21] Y. Peng, J.H. Li, W.Z. Si, X. Li, W.B. Shi, J.M. Luo, J. Fu, J. Crittenden, J.M. Hao, Chem. Eng. J. 269 (2015) 44–50.
[22] L. Yang, Y. Tan, Z.Y. Sheng, A.Y. Zhou, J. Nanomater. 2014 (2014) 1–6.
[23] R.B. Jin, Y. Liu, Y. Wang, W.L. Cen, Z.B. Wu, H.Q. Wang, X.L. Weng, Appl. Catal. B: Environ. 148–149 (2014) 582–588.
[24] L.J. Zhang, S.P. Cui, H.X. Guo, X.Y. Ma, X.G. Luo, J. Mol. Catal. A: Chem. 390 (2014) 14–21.
[25] R. Zhang, Q. Zhong, W. Zhao, Res. Chem. Intermed. 41 (2015) 3479–3490.
[26] S.L. Zhang, Q. Zhong, W. Zhao, Y.T. Li, Chem. Eng. J. 253 (2014) 207–216.
[27] S.L. Zhang, H.Y. Li, Q. Zhong, Appl. Catal. A: Gen. 435–436 (2012) 156–162.
[28] H.Q. Wang, S. Cao, Z. Fang, F.X. Yu, Y. Liu, X.L. Weng, Z.B. Wu, Appl. Surf. Sci. 330 (2015) 245–252.
[29] K.J. Zhen, G.J. Wang, Y.L. Bi, R.S. Li, Catal. Basis, 3rd ed., Science Press, Beijing, 2005.
[30] Y.S. Shen, Y.F. Ma, S.M. Zhu, Catal. Sci. Technol. 2 (2012) 589–599.
[31] L.J. Liu, Y.Q. Jiang, H.L. Zhao, J.T. Chen, J.L. Cheng, K.S. Yang, Y. Li, ACS Catal. 6 (2016) 1097–1108.
[32] J.G. Yu, J.X. Low, W. Xiao, P. Zhou, M. Jaroniec, J. Am. Chem. Soc. 136 (2014) 8839–8842.
[33] K.L. Lv, Q.J. Xiang, J.G. Yu, Appl. Catal. B: Environ. 104 (2011) 275–281.
[34] W. Wang, C.H. Lu, Y.R. Ni, M.X. Su, Z.Z. Xu, Appl. Catal. B: Environ. 127 (2012) 28–35.
[35] W. Wang, C.H. Lu, Y.R. Ni, Z.Z. Xu, CrystEngComm 15 (2013) 2537–2543.
[36] H.G. Yang, C.H. Sun, S.Z. Qiao, J. Zou, G. Liu, S.C. Smith, H.M. Cheng, G.Q. Lu, Nature 453 (2008) 634–638.
[37] R. Fernández-González, B. Julián-López, E. Cordoncillo, P. Escribano, J. Mater. Chem. 21 (2011) 497–504.
[38] X.R. Li, J.G. Wang, Y. Men, Z.F. Bian, Appl. Catal. B: Environ. 187 (2016) 115–121.
[39] L. Lietti, I. Nova, E. Tronconi, P. Forzatti, Catal. Today 45 (1998) 85–92.
[40] P. Ning, Z.X. Song, H. Li, Q.L. Zhang, X. Liu, J.H. Zhang, X.S. Tang, Z.Z. Huang, Appl. Surf. Sci. 332 (2015) 130–137.
[41] Y. Jiang, Z.M. Xing, X.C. Wang, S.B. Huang, X.W. Wang, Q.Y. Liu, Fuel 151 (2015) 124–129.
[42] X. Gao, Y. Jiang, Y.C. Fu, Y. Zhong, Z.Y. Luo, K.F. Cen, Catal. Commun. 11 (2010) 465–469.
[43] H.Q. Zhu, Z.F. Qin, W.J. Shan, W.J. Shen, J.G. Wang, J. Catal. 225 (2004) 267–277.
[44] B. Murugan, A.V. Ramaswamy, J. Phys. Chem. C 112 (2008) 20429–20442.
[45] Q.L. Zhang, X. Liu, P. Ning, Z.X. Song, H. Li, J.J. Gu, Catal. Sci. Technol. 5 (2015) 2260–2269.
[46] M.E. Yu, C.T. Li, G.M. Zeng, Y. Zhou, X.N. Zhang, Y.E. Xie, Appl. Surf. Sci. 342 (2015) 174–182.
[47] Y. Liu, P.F. Fang, Y.L. Cheng, Y.P. Gao, F.T. Chen, Z. Liu, Y.Q. Dai, Chem. Eng. J. 219 (2013) 478–485.
[48] M.Y. Smirnov, G.W. Graham, Catal. Lett. 72 (2001) 39–44.
[49] Z.B. Wu, R.B. Jin, Y. Liu, H.Q. Wang, Catal. Commun. 9 (2008) 2217–2220.
[50] T. Tachikawa, S. Yamashita, T. Majima, J. Am. Chem. Soc. 133 (2011) 7197–7204.